NASA/TP-2005-213528

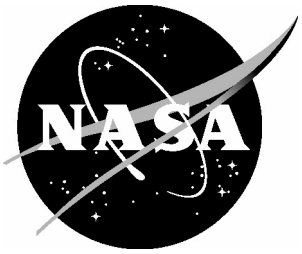

Turbulence Hazard Metric Based on Peak Accelerations for Jetliner Passengers

Eric C. Stewart
Langley Research Center, Hampton, Virginia

February 2005

The NASA STI Program Office . . . in Profile

Since its founding, NASA has been dedicated to the advancement of aeronautics and space science. The NASA Scientific and Technical Information (STI) Program Office plays a key part in helping NASA maintain this important role.

The NASA STI Program Office is operated by Langley Research Center, the lead center for NASA's scientific and technical information. The NASA STI Program Office provides access to the NASA STI Database, the largest collection of aeronautical and space science STI in the world. The Program Office is also NASA's institutional mechanism for disseminating the results of its research and development activities. These results are published by NASA in the NASA STI Report Series, which includes the following report types:

- TECHNICAL PUBLICATION. Reports of completed research or a major significant phase of research that present the results of NASA programs and include extensive data or theoretical analysis. Includes compilations of significant scientific and technical data and information deemed to be of continuing reference value. NASA counterpart of peer-reviewed formal professional papers, but having less stringent limitations on manuscript length and extent of graphic presentations.

- TECHNICAL MEMORANDUM. Scientific and technical findings that are preliminary or of specialized interest, e.g., quick release reports, working papers, and bibliographies that contain minimal annotation. Does not contain extensive analysis.

- CONTRACTOR REPORT. Scientific and technical findings by NASA-sponsored contractors and grantees.

- CONFERENCE PUBLICATION. Collected papers from scientific and technical conferences, symposia, seminars, or other meetings sponsored or co-sponsored by NASA.

- SPECIAL PUBLICATION. Scientific, technical, or historical information from NASA programs, projects, and missions, often concerned with subjects having substantial public interest.

- TECHNICAL TRANSLATION. English-language translations of foreign scientific and technical material pertinent to NASA's mission.

Specialized services that complement the STI Program Office's diverse offerings include creating custom thesauri, building customized databases, organizing and publishing research results ... even providing videos.

For more information about the NASA STI Program Office, see the following:

- Access the NASA STI Program Home Page at ***http://www.sti.nasa.gov***

- E-mail your question via the Internet to help@sti.nasa.gov

- Fax your question to the NASA STI Help Desk at (301) 621-0134

- Phone the NASA STI Help Desk at (301) 621-0390

- Write to:
  NASA STI Help Desk
  NASA Center for AeroSpace Information
  7121 Standard Drive
  Hanover, MD 21076-1320

NASA/TP-2005-213528

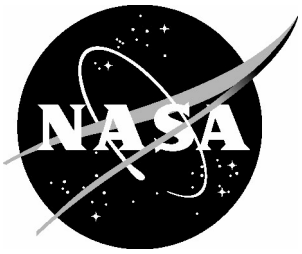

Turbulence Hazard Metric Based on Peak Accelerations for Jetliner Passengers

Eric C. Stewart
Langley Research Center, Hampton, Virginia

National Aeronautics and
Space Administration

Langley Research Center
Hampton, Virginia 23681-2199

February 2005

Available from:

NASA Center for AeroSpace Information (CASI)
7121 Standard Drive
Hanover, MD 21076-1320
(301) 621-0390

National Technical Information Service (NTIS)
5285 Port Royal Road
Springfield, VA 22161-2171
(703) 605-6000

Abstract

Calculations are made of the approximate hazard due to peak normal accelerations of an airplane flying through a simulated vertical wind field associated with a convective frontal system. The calculations are based on a hazard metric developed from a systematic application of a generic math model to 1-cosine discrete gusts of various amplitudes and gust lengths. The math model simulates the three degree-of-freedom longitudinal rigid body motion to vertical gusts with simplified expressions for (1) fuselage flexibility, (2) the lag in the downwash from the wing to the tail, (3) gradual lift effects, (4) an autopilot, and (5) motion of an unrestrained passenger in the rear cabin. Airplane and passenger response contours are calculated for a matrix of gust amplitudes and gust lengths. The airplane response contours are used to develop an approximate hazard metric of peak normal accelerations as a function of gust amplitude and gust length. The hazard metric is then applied to a two-dimensional simulated vertical wind field of a convective frontal system. The variations of the hazard metric with gust length and airplane heading are demonstrated.

Introduction

The National Aeronautics and Space Administration (NASA) has initiated an aviation safety program aimed at reducing the accident rate of transport airplanes. One element of this program concerns the injuries and fatalities caused by encounters with turbulence. Although there have been many studies on airplane gust loads, these studies have primarily been concerned with the structural integrity of the airplanes and the resulting certification issues. However, in most accident scenarios, the airplane structure is not damaged, but flight attendants and unrestrained passengers are injured or killed (ref. 1). Often the airplane unexpectedly encounters a discrete gust of only a few seconds' duration while flying in otherwise relatively calm air. A study that specifically addresses the transient responses of airplanes to realistic turbulence is needed. For example, the critical gust amplitudes and gust lengths that induce accidents need to be identified. Once these parameters are known, forward-looking sensors such as radar and lidar can be better designed to detect and avoid dangerous gusts.

A three-step procedure is used to study these factors. First, a simulation math model is developed to explore the responses of both the airplane and unrestrained passengers to gusts of various shapes and sizes. This model is generic with minimal airplane characteristics. However, the model includes representations of such things as nonlinear aerodynamics of the wing, a simple autopilot, rear fuselage bending, the lag in the downwash from the wing to the tail, gradual lift effects on the wing, and inelastic collisions of an unrestrained object with the interior of the rear cabin. This model was first described in reference 2. Although the model structure is generic, for this study the parameters in the model are limited to a single configuration for a medium range jetliner.

The second step is to develop an algorithm to predict peak normal accelerations for a given vertical gust profile. A preliminary version of the algorithm is described in reference 3. The present algorithm is believed to be more accurate and easier to implement. It is developed by calculating the transient response to a 1-cosine gust for a matrix of gust amplitudes and gust lengths at a cruise flight condition. To make the results more applicable to other airplane configurations and flight conditions, the gust

amplitudes and gust lengths are nondimensionalized by using airplane response factors. Next, an approximate acceleration equation is fitted to the nondimensionalized data. This acceleration equation is then used in the hazard metric algorithm to predict the peak normal acceleration for an arbitrary gust profile. The algorithm first calculates the approximate incremental gust amplitude for the given gust profile for five different gust lengths spanning the estimated range of interest. Then the approximate gust amplitude and gust length are substituted into the acceleration equation to predict the peak normal acceleration for each of the five gust lengths. The two peak accelerations (positive and negative) for all five gust lengths are defined as the hazard.

The third and final step is to apply the hazard algorithm and acceleration equation to a simulated wind field as an example. The wind field was generated by using NASA's Terminal Area Simulation System (TASS), a large eddy simulation of atmospheric convection (ref. 4). The application of the acceleration equation to the simulated wind field produces the two peak accelerations as a function of the assumed gust lengths. This analysis gives an indication of the gust lengths that are most likely to be a hazard to airplanes. Also, the effect of changing the direction of flight through the same wind field is investigated.

Nomenclature

A nondimensional gust amplitude

A' dimensional gust amplitude, ft/s

a_{aft} normal force factor at aft passenger cabin (eq. (24), positive upward), ft/s^2

alt altitude, ft

a_n peak normal acceleration at aft cabin location, g's

$(a_n)^+$ peak positive acceleration from hazard metric algorithm, g's

$(a_n)^-$ peak negative acceleration from hazard metric algorithm, g's

a_z z-force factor (eq. (4), positive downward), ft/s^2

$C_{D,i}$ total drag coefficient of ith surface, nondimensional

$C_{Do,t}$ zero lift drag coefficient of tail, nondimensional

$C_{L,i}$ lift coefficient of ith surface, nondimensional

$C_{L,\alpha}$ lift curve slope of airplane, per rad

$C_{L\alpha,t}$ lift curve slope of tail, per rad

c_w mean aerodynamic chord of wing, ft

d_{fall} equivalent fall height in 1-g gravity field (see (eq. 28)), ft

F_s force due to flexible fuselage spring, lb

$F_{x,i}$ component of force along X-body axis ($i = w, t, T$), lb

$F_{z,i}$ component of force along Z-body axis ($i = w, t, ta, T$), lb

f frequency of flexible fuselage mode, 3 Hz

g acceleration of gravity, 32.2 ft/s^2

h position of unrestrained mass above aft cabin floor, ft

$\dot{h}_c$ collision velocity of unrestrained mass with floor or ceiling, ft/s

I_y moment of inertia about y (pitch) axis, slug-ft^2

k flexible fuselage spring constant, lb/ft

k_h altitude hold feedback gain in autopilot, rad/ft

k_q pitch rate gain in autopilot, rad/(rad/s)

k_t efficiency factor of tail, nondimensional

$k_{\delta e}$ elevator effectiveness, nondimensional

k_θ pitch angle gain in autopilot, rad/rad

L nondimensional gust length

L' dimensional gust length, m or ft

m mass of wing body, slugs

m_e equivalent mass of aeroelastic tail structure, slugs

$m_{i,j}$ least-squares slope for ith gust length and jth measurement, (ft/s)/ft

Δn_{aft} delta normal acceleration of aft passenger cabin, g's

Δn_{cg} delta normal acceleration of center of gravity, g's

q pitch rate, rad/s

$\bar{q}$ dynamic pressure, psf

R_c ratio of longitudinal cabin position to tail length = 0.8 (eq. (24)), nondimensional

R_s ratio of structural tail deflection to tail length = 0.02 (eq. (12)), nondimensional

S_t horizontal tail area, 542 ft^2

S_w wing area, 1951 ft^2

t time, s

Δt lag in wing downwash reaching tail, s

u_g component of gust velocity along X-body axis positive aft, ft/s

u_o component of inertial velocity along X-body axis, ft/s

u_w component of true airspeed along X-body axis at wing, ft/s

V true airspeed, ft/s

W weight of airplane, lb

w_g vertical gust velocity positive up, ft/s or m/s

$(w_g')_j$ jth measurement of vertical gust velocity, ft/s

w_o component of inertial velocity along Z-body axis, ft/s

w_w component of true airspeed along Z-body axis at wing, ft/s

w_x horizontal gust velocity along X-Earth axis, positive aft, ft/s

w_z component of gust velocity along Z-Earth axis, positive up, ft/s

x position of airplane center of gravity along X-Earth axis (eq. (31)), ft

x_i x location of point of application of ith force component, ft

x_j x position of airplane for jth measurement, ft

x_t location of tail aerodynamic center in body axis system, ft

x_w location of wing aerodynamic center in body axis system, ft

y_{trim} vertical displacement of horizontal tail due to aeroelastic effects at trim flight condition, ft

z_i z location of point of application of ith force component, ft

α angle of attack, rad or deg

Δy change in length of spring from trim length, ft

δ_{ap} elevator deflection due to autopilot, rad

δ_e elevator deflection, rad or deg

δ_{ec} commanded elevator deflection due to simulated autopilot, rad

$\frac{\partial \varepsilon}{\partial \alpha}$ downwash parameter, nondimensional

η inclination of thrust axis with respect to x-body axis (positive up), rad

θ pitch angle, rad/deg

ρ density of air, slug/ft^3

σ_n standard deviation of normal acceleration, *g*'s

σ'_w standard deviation of vertical gust velocity, ft/s

Subscripts:

aft in aft passenger cabin

b body (axis system)

e Earth (axis system)

g gust

i *i*th aerodynamic component or *i*th measurement in hazard algorithm

T thrust

t (horizontal) tail

trim at trim flight condition

ta (horizontal) tail aerodynamic

w wing

Operators:

Δ change

. first derivative with respect to time

.. second derivative with respect to time

$f_D()$ nonlinear wing drag function

$f_L()$ nonlinear wing lift function

Abbreviations:

ac aerodynamic center

c.g. center of gravity

NASA National Aeronautics and Space Administration

TASS Terminal Area Simulation System

Simulation Description and Results

Math Model

The equations of motion are written in a body axis system that is free to translate and pitch in a vertical plane. The airplane is modeled as a wing-body mass connected by a spring to the effective horizontal tail mass. The airplane mass is acted on by the wing-body aerodynamic forces, gravity forces, thrust forces, the X aerodynamic force of the horizontal tail, and a Z tail force produced by the connecting spring. The Z aerodynamic tail force, the connecting spring force, and gravity act on the effective tail mass. A diagram of the model is presented in figure 1. The equations of motion for this system are given below.

Airplane wing body:

$$\sum_i F_{x,i} - mg\sin(\theta) = m(\dot{u}_o + qw_o) \tag{1}$$

$$\sum_i F_{z,i} + mg\cos(\theta) = m(\dot{w}_o - qu_o) \tag{2}$$

$$\sum_i F_{x,i} z_i - \sum_i F_{z,i} x_i = I_y \dot{q} \tag{3}$$

where $i = w,t,T$.

Flexible tail:

$$\Delta\ddot{y} = \frac{F_s}{m_e} + \frac{F_{z,ta}}{m_e} - a_z - g + x_t\dot{q} \tag{4}$$

where

$$a_z = \frac{\sum_i F_{z,i}}{m}$$

The X aerodynamic forces for the wing and tail in equations (1) and (3) are derived from the lift and drag

$$F_{x,i} = \bar{q}S_i[-C_{D,i}\cos(\alpha_i) + C_{L,i}\sin(\alpha_i)] \tag{5}$$

where $i = w,t$ with the nonlinear, table-lookup aerodynamic characteristics of the wing (see fig. 2):

$$\left.\begin{aligned} C_{L,w} &= f_L(\alpha_w) \\ C_{D,w} &= f_D(\alpha_w) \end{aligned}\right\} \tag{6}$$

Note that a stall break was not simulated for negative angles of attack because of a lack of reliable aerodynamic data in that region. The estimated aerodynamic characteristics of the tail were

$$\left.\begin{aligned} C_{L,t} &= C_{L\alpha,t}\alpha_t \\ C_{D,t} &= C_{Do,t} + k_t C_{L,t}^2 \end{aligned}\right\} \tag{7}$$

The force components for the thrust are

$$F_{x,T} = \text{Thrust} * \cos(\eta) \tag{8}$$

$$F_{z,T} = -\text{Thrust} * \sin(\eta) \tag{9}$$

The aerodynamic Z forces for the wing and the elastic tail are

$$F_{z,i} = \bar{q} S_i [-C_{L,i} \cos(\alpha_i) - C_{D,i} \sin(\alpha_i)] \tag{10}$$

where $i = w,ta$.

The Z force from the tail $(F_{Z,t})$ that is transmitted to the wing body through the simulated spring is not the same as the aerodynamic tail force $(F_{z,ta})$ given in equation (10). It is, instead, equal and opposite F_s in equation (4):

$$F_{Z,t} = -F_s = -k(y_{trim} + \Delta y) \tag{11}$$

The spring constant, k, in equation (11) and the effective tail mass, m_e, in equation (4) were estimated as follows. First, a natural frequency of the elastic tail system was assumed; that is, f = 3 Hz, which is a reasonable value for a medium range jetliner. Then a structural stiffness was calculated by assuming that the tail would deflect a given ratio, $R_s = 0.02$, of the tail length if loaded with the entire weight of the wing body. That is,

$$k = (mg) / (-x_t * R_s) \tag{12}$$

The value $R_s = 0.02$ is consistent with unpublished estimates of the change in horizontal tail incidence due to structural deformation for a medium range jetliner. Finally, the effective mass is calculated from the spring constant and the assumed natural frequency

$$m_e = \frac{k}{(2\pi f)^2} \tag{13}$$

The angles of attack on the wing and tail are, of course, critical to the proper calculations of the aerodynamic forces and moments. The angle of attack at the wing was calculated from the following equation:

$$\alpha_w = \tan^{-1}\left(\frac{w_w}{u_w}\right) \tag{14}$$

in which the velocity components for the wing are a straightforward sum of the inertial components and the gust components

$$u_w = u_o + u_g \tag{15}$$

$$w_w = w'_o + w'_g \tag{16}$$

The primed parameters are the gradual lift effects represented by the approximate formulas (ref. 5):

$$\left.\begin{aligned} w'_o &= w_o\left(1 - 0.36e^{-t/\tau_o}\right) \\ w'_g &= w_g\left(1 - e^{-t/\tau_g}\right) \end{aligned}\right\} \tag{17}$$

with

$$\left.\begin{aligned} \tau_o &= \frac{3c_w}{2V} \\ \tau_g &= \frac{3c_w}{4V} \end{aligned}\right\} \tag{18}$$

The velocity components for the tail are more complicated (eqs. (19) and (20)), even though gradual lift effects are ignored because of the smaller size of the tail and the shorter time constants due to the shorter chord of the tail. For example, the gust hits the tail slightly after it hits the wing; see the $u_g(t-\Delta t)$ and $w_g(t-\Delta t)$ terms in equations (19) and (20), respectively. Also, the downwash from the wing modifies the velocity at the tail; see the $\left(1-\frac{\partial\varepsilon}{\partial\alpha}\right)$term in equation (20). Of course, the pitching motion of the airplane induces a vertical velocity ($-x_t q$ in eq. (20)) at the tail that is primarily responsible for the pitch damping (ref. 6). Adding the flexible tail degree of freedom adds more terms to these basic effects. The vertical motion of the elastic tail induces a vertical velocity component at the tail ($\Delta\dot{y}$ in eq. (20)) that is responsible for the damping of this structural mode.

$$u_t = u_o + u_g(t-\Delta t) + z_t * q \tag{19}$$

$$w_t = w_o - \frac{\partial\varepsilon}{\partial\alpha}w_o(t-\Delta t) + \left(1-\frac{\partial\varepsilon}{\partial\alpha}\right)w_g(t-\Delta t) - x_t q + \Delta\dot{y} \tag{20}$$

where the $(t-\Delta t)$ notation indicates the parameter is evaluated at an earlier time (with $\Delta t = (x_w - x_t)/V$) to account for the time difference in effects at the tail and the wing. All other parameters are evaluated at the current time *t*.

The angle of attack at the tail was calculated from the previously mentioned velocity components plus two additional terms:

$$\alpha_t = \tan^{-1}\left(\frac{w_t}{u_t}\right) + k_{\delta_e}\delta_e + \frac{2(\Delta y + y_{trim})}{-x_t} \tag{21}$$

The second term on the right-hand side of equation (21) is the effect of the elevator (used from trimming the simulated airplane and as the autopilot effector), while the third term is the change in angle of attack due to the structural deflection of the rear fuselage. The factor of 2 arises from the assumption that the fuselage deflection is proportional to the square of the distance from the center of gravity.

The autopilot control law contained feedback terms for the pitch rate, pitch attitude, and altitude:

$$\delta_{ec} = k_q q + k_\theta(\theta - \theta_{trim}) + k_h(alt - alt_{trim}) \tag{22}$$

This commanded elevator was passed through a 14-rad/s first-order actuator model to produce the autopilot output, δ_{ap}, which was added to the trimmed elevator position

$$\delta_e = \delta_{ap} + \delta_{e,trim} \tag{23}$$

To simulate the collisions of an unrestrained passenger with the ceiling and floor, an auxiliary calculation was made. The first step was to calculate the normal acceleration at an estimated extreme aft cabin position

$$a_{\text{aft}} = -a_z + (R_c)x_t\dot{q} - (R_c)^2\Delta\ddot{y} \tag{24}$$

where $R_c = 0.8$ was the estimated ratio of the aft cabin location to the tail location, x_t. The ratio is squared in the third term because the structural deflection curve of the rear fuselage was assumed to be quadratic. Whenever the unrestrained body (passenger) was not in contact with either the floor or the ceiling $(0 < h < 4)$, its acceleration relative to the (accelerating) cabin floor or ceiling was

$$\ddot{h} = -a_{\text{aft}} \tag{25}$$

This acceleration was then integrated to produce the relative velocity and position. Inelastic collisions with the floor and ceiling were simulated by setting $\dot{h} = 0$ whenever

$$h \le 0 \text{ and } (\dot{h} < 0 \text{ or } \ddot{h} < 0) \tag{26}$$

or

$$h \ge 4 \text{ and } (\dot{h} > 0 \text{ or } \ddot{h} > 0) \tag{27}$$

so that there was no rebound of the passenger from the interior boundaries of the cabin.

The 4 (ft) constant in equation (27) was a compromise between (1) the distance between a passenger's head while standing in the aisle and the ceiling and (2) the much longer distance from the ceiling to the floor. After the instantaneous velocity, $\dot{h}_c$, at the time the body collided with either the floor or the ceiling was determined, it was transformed into an equivalent height of a fall in a normal 1-g gravity field by using

$$d_{fall} = \frac{\left(\dot{h}_c + V_a\right)^2}{2\mathrm{g}} \tag{28}$$

where V_a is an approximate term added to account for the fact that the floor (or ceiling) is either accelerating away from or toward the passenger when he impacts the floor (or ceiling).

$$V_a = +4\sqrt{\left|\Delta n_{\mathrm{aft}}\right|}\,\mathrm{sign}\left(-\Delta n_{\mathrm{aft}}\right) \tag{29}$$

The constant of 4 (ft/s) is based on the assumption that the body of the passenger deforms 3 in. upon impact, $s = \frac{3}{12}$ ft, according to the following equation:

$$\left|V_a\right| = +\sqrt{2as} = +\sqrt{(2)\left(32 * \left|\Delta n_{\mathrm{aft}}\right|\right)\left(\frac{3}{12}\right)} = +\sqrt{16 * \left|\Delta n_{\mathrm{aft}}\right|} = +4\sqrt{\left|\Delta n_{\mathrm{aft}}\right|} \tag{30}$$

Gust inputs

A 1-cosine gust profile was used to excite the previous math model. The equation used to produce the vertical wind was

$$w_g = \left(\frac{A'}{2}\right)\left[1 - \cos\left(\frac{\pi}{L'}\right)x\right] \tag{31}$$

where x is the x position of the airplane in the Earth axis system, A' is the dimensional gust amplitude, and L' is the dimensional gust length. A plot of the 1-cosine gust profile for typical values of A' and L' is shown in figure 3 as a function of time.

A 1-cosine gust profile was used because it contains the fundamental characteristics of turbulence that excite airplanes—the incremental amplitude and the distance over which the incremental amplitude changes. That is, the acceleration of an airplane to a given incremental amplitude gust will increase the faster the change in the gust occurs. The 1-cosine gust profile also approximates a discrete gust rather than continuous, random turbulence. Large, discrete gusts are what cause most in-flight injuries (ref. 7).

Simulated Responses to 1-Cosine Gusts

The previous equations were translated into a Matlab® Simulink® block diagram for solution. The model was trimmed to a cruise flight condition (Mach = 0.8 at 30 000 ft) by an iterative routine that determined the trim thrust, angle of attack, elevator position, and spring deflection to produce zero accelerations in level flight. The simulated airplane characteristics are presented in table 1. These characteristics represent a medium range jetliner that can carry approximately 200 passengers.

Time histories of the simulated transient response to a large, downward gust starting at approximately 2.5 s are shown in figure 4. The maximum change in angle of attack was about −7° (for a gust amplitude

of −150 ft/s), which did not stall the wing because its initial trim angle of attack was slightly more than +1°. However, as will be shown later, an upward gust of the same magnitude will stall the wing. The normal acceleration at the c.g., Δn_{cg}, and the acceleration at the aft passenger location, Δn_{aft}, are practically equal because the illustrated gust length of 1000 ft is so long that the pitching motion, $\Delta\theta$, is relatively slow. As will be shown later, for shorter gust lengths, the acceleration at the aft passenger location is considerably higher than that at the center of gravity.

The change in true airspeed, ΔV, was much less than the maximum gust velocity of 150 ft/s because the latter was nearly perpendicular to the true airspeed of approximately 800 ft/s. The structural deflection of the horizontal tail, Δy, was relatively small (less than 0.2 ft), indicating that the simulated airplane was relatively stiff. Because the change in the acceleration in the aft cabin dropped below −1g, the simulated passenger came off the floor and impacted the 4-ft ceiling at approximately 3.5 s into the time history (see the time history of h). The relative velocity at impact was approximately 20 ft/s (see $\dot{h}$); however, after the acceleration reversed at about 4.2 s, the simulated passenger fell back down to the floor with slightly greater impact velocity than that for the first impact.

Response Contours

A matrix of gust lengths and gust amplitudes was run through the simulation program to produce time histories. A second program then extracted the maximum values of the accelerations, passenger impact velocities, and equivalent fall heights. These data were then transformed into contour plots such as those shown in figure 5 for the equivalent fall heights of the unrestrained mass (simulated passenger). The maximum contours occur for gust lengths of approximately 500 ft. However, they drop off sharply for the smallest gust lengths even though the aft cabin accelerations were very high for short gust lengths, as will be shown next. The reason for these dropoffs is that for the shorter gust lengths, the accelerations were sustained for such short periods of time that the resulting velocities and displacements of the simulated passenger were relatively small. In fact, for the shorter gusts the simulated passengers did not impact the ceiling at all, but only came off the floor a small distance before impacting with the floor again.

Figure 6 presents the contour plots for the normal acceleration at the c.g. As can be seen in the figure, the maximum accelerations are a function of both the gust length and the gust amplitude. For example, at a gust amplitude of −50 ft/s, the acceleration varies from −1.0 g's at a gust length of about 600 ft to only −0.5 g's at a gust length of about 2400 ft. However, at very short gust lengths, the accelerations drop off again because of the gradual lift effects used in the simulation. Note that for positive gusts greater than about 100 ft/s, the accelerations are smaller than the absolute value of accelerations for negative gusts because the wing begins to stall, reducing the lift. As seen in figure 2, the lift curve slope begins to decrease at about $\alpha = 5°$ and reaches a maximum at about $\alpha = 7°$. Since the trim angle of attack was over 1°, the acceleration due to the gust would begin to increase less rapidly whenever the gust-induced angle of attack was over 4° (approximately 60 ft/s). As mentioned earlier, nonlinear stall effects were not modeled for negative angles of attack because of a lack of reliable aerodynamic data in this region; therefore, the accelerations in the negative direction may be too large for large negative gusts. From a hazard standpoint, however, these negative acceleration results would be conservative.

The contour plots for the normal acceleration at the aft cabin location (fig. 7) are practically identical to those at the center of gravity for gust lengths greater than 1000 ft. However, at the shorter wavelengths, the aft cabin accelerations are significantly higher. Part of this increase is due to the pitching motion of the simulated airplane, but a significant part is due to the excitation of the structural mode of

the tail. The combined effect of the pitching and structural mode is enough to offset most of the reduction caused by the gradual lift effects.

Algorithm Development

Approximate Acceleration Response Equation

The contour plots for the normal acceleration at the aft cabin location (fig. 7) were nondimensionalized to make them more generally applicable to other airplane configurations and flight conditions (fig. 8). The gust amplitude was nondimensionalized by dividing by the factor $\frac{2 \text{ Weight}}{\rho S V C_{L_\alpha}}$, which represents the amplitude of a step gust that would produce a 1-g acceleration. As can be seen in figure 8, the y intercepts of the ±1-g contours are approximately ±1, confirming the consistency of the present analysis. The gust length was nondimensionalized by dividing by the factor $\frac{2m}{\rho S C_{L_\alpha}}$, which represents the forward distance traveled by the airplane in one time constant of the airplane's plunge mode.

To develop a general expression for the hazard metric, a straight-line approximation was fit to the contours in figure 8. The straight line that was determined was

$$A = 0.96 * a_n + 0.70 * a_n * L \tag{32}$$

where A and L are the nondimensional gust amplitudes and gust lengths, respectively. This equation can be solved for the (peak aft cabin) acceleration, a_n,

$$a_n = \frac{A}{0.96 + 0.70 * L} \tag{33}$$

It can be seen from figure 9 that the curve fits the contours better for negative gust amplitudes than for positive amplitudes, again because of the stalling of the wing for positive amplitudes. The lack of fit for positive amplitudes is in a conservative direction because the curve predicts higher accelerations than the accelerations of the contour lines (e.g., +2.0-g contour).

Hazard Algorithm

Of course, physical gusts do not generally have 1-cosine shapes; therefore, it might seem impossible to apply this curve fit to real gusts. However, real gusts can be approximated by a series of 1-cosine gusts with different gust amplitudes and gust lengths. In this study a least-squares linear fit was used to calculate the running incremental gust amplitudes for five different gust lengths (see fig. 10). The gust lengths were selected so as to span the wavelengths that airplanes are most responsive to −50 m (160 ft) to 800 m (2600 ft). To calculate the approximate peak accelerations at the aft cabin location, the incremental gust amplitudes were then inserted into equation (33) for each gust length.

A proposed operational algorithm for a turbulence hazard metric is shown in figure 11. The proposed metric actually consists of three numbers: the standard deviation of the acceleration, σ_n, the positive peak acceleration $(a_n)^+$, and the negative peak acceleration, $(a_n)^-$. The metric could be reported to pilots as, for example, "Turbulence is 0.2 g's continuous (σ_n), with peaks to +0.5 g's ($(a_n)^+$) and

−0.7 g's ($(a_n)^-$)." Because the peak acceleration, regardless of gust length, may be the critical metric (ref. 8), the maximum and minimum accelerations for all five gust lengths combined are reported as shown in figure 11. In fact, the peak negative accelerations are probably the most critical because if they become more negative than −1 g, unrestrained passengers will be thrown into the ceiling and then eventually back to the floor where they sustain most of their injuries.

Application to a Simulated Wind Field

Simulated Wind Field

Figure 12 contains a contour plot of vertical gust velocities in a convective frontal system as simulated by TASS (ref. 4). The gust velocities were calculated on a two-dimensional grid with a 25-m (82-ft) spacing in each direction. The plot shows that there are concentrated areas of upward and downward gust velocities relatively close to each other. The finer detail of the gust field illustrated in figure 13 shows the vertical gust velocities on two parallel lines 25 m (82 ft) apart. There are significant differences even this close together; thus, it would seem that if this simulated gust field is realistic, two identical airplanes flying close together would experience significant differences in the accelerations produced.

Approximate Acceleration Equation Validation

Figure 14 shows time histories of a full, six-degree-of-freedom nonlinear simulation of a passenger transport airplane flying through the simulated turbulence field. The trajectory is approximately along the same line as the one in figure 13(a); however, because the simulated airplane was not constrained to a given line, the gust velocities encountered were not exactly the same. The simulated peak accelerations were approximately ±0.4 g's from the nominal +1 g.

The time histories in figure 14 can be compared to the predicted approximate peak accelerations for the 100-m (330-ft) gust length shown in figure 15. The predicted approximate peak accelerations are, of course, not theoretically the same as the instantaneous accelerations of figure 14. Only the peak values of the instantaneous accelerations should correspond to the peak values predicted by the hazard algorithm. An operational hazard algorithm (fig. 11) would produce the peaks of all five gust lengths combined, not just the 100-m (330-ft) gust length used to produce figure 15. However, as will be shown later, the 100-m (330-ft) gust length produced some of the largest peak accelerations. In any case, the predicted incremental peak accelerations in figure 15 are about ±0.4 g's, which are in good agreement with the peaks in figure 14.

Acceleration Contours

Contours of the maximums and minimums for all five gust lengths combined are shown in figures 16(a) and (b), respectively. The peak positive acceleration was +1.50 g's and the peak negative acceleration was −1.78 g's. A comparison of the figures indicates the areas of maximum and minimum accelerations are often very close together as a result of the proximity of the up and down gusts previously discussed for figure 12.

Acceleration contours for the five individual gust lengths are shown in figures 17(a) through (e). Although the numerical values of the contours are different for the different gust lengths, the general pattern of the contours is relatively constant. The numerical values of the accelerations are generally larger for the smaller gust lengths, indicating that the shorter gust lengths are the most hazardous.

The acceleration contours in figure 17 are for airplane trajectories traveling from left to right or a heading of zero. However, the accelerations at any point are generally a function of the heading the airplane flies through the turbulence field. The differences in the acceleration for headings of 30°, 60°, and 90° are shown in figure 18 for the 100-m (330-ft) gust length. These figures can be compared to the corresponding figure 17(b) which is for a heading of 0°. A close examination of individual points in the contour shows substantial differences. For example, the maximum acceleration of 1.42 g's in figure 17(b) occurs at x = 4675 m, and y = 4100 m. The corresponding accelerations at the same point in figure 18 are given in the following chart:

Maximum accelerations at x = 4675 m, y = 4100 m

Heading, deg	0	30	60	90
Acceleration, g's	1.42	0.53	0.14	0.37

The differences in the fine detail mean that airplanes flying through the same point in the turbulence field can experience significantly different accelerations depending on the heading. However, as will be shown in the next section, the peak accelerations over the entire 256 by 256 points are relatively unaffected by the heading.

Effect of Gust Length and Airplane Heading on Peak Accelerations

The effect of gust length on the peak accelerations is summarized in figure 19. As mentioned earlier, the peak accelerations are generally larger for shorter gust lengths. The peak minimum acceleration appears to reach a minimum at a gust length of 100 m, but this appearance may be due to the single data point at a gust length of 50 m. In any case, if the simulated turbulence field is realistic, this analysis would indicate that the largest accelerations are produced by gust lengths of 100 to 50 m (330 to 160 ft) or less. This result is supported by actual flight data taken during a NASA research flight for the same class of airplane as that used in the analysis. This flight took place in the actual weather system that the present simulated wind field was designed to model. The largest "hit" in the flight test produced peak changes in the vertical acceleration of +0.81 g's and −1.35 g's. The −1.35-g acceleration occurred when there was a near step change in the vertical gust velocity of −55 ft/s (17 m/s) over a distance of approximately 64 ft (20 m). It is probable that this gust induced a significant structural response.

Note that since the simulated gust field had a grid spacing of 25 m, the shortest practical gust length in this study was 50 m; that is, only 3 points in the grid were used to calculate the incremental gust amplitudes for the 50-m gust length. Gust lengths of less than 50 m could not be analyzed; therefore, a finer grid is needed to establish the value of the gust length that produces the largest accelerations. The peak accelerations for gust lengths of less than 50 m need to be determined to see whether the curves in figure 19 have a local maximum or minimum. However, as discussed earlier in relation to the equivalent fall heights of unrestrained passengers shown in figure 5, the gust lengths most hazardous to unrestrained passengers may be much higher—on the order of 500 ft. As mentioned earlier, the shorter gust lengths, although producing large accelerations, act for such a short period of time that the equivalent fall heights are smaller. A hazard metric based on equivalent fall heights would be fundamentally different from the present hazard metric based on accelerations.

The effect of airplane heading on the peak accelerations is summarized in figure 20. It appears that variations in the peak accelerations over the entire grid are relatively small and insignificant. However, as shown earlier, the differences at a given location can be significant.

Concluding Remarks

A turbulence hazard metric has been developed based on the transient acceleration response of a medium-sized jetliner to a 1-cosine gust at a cruise flight condition. To make the hazard metric more applicable to other jetliners and flight conditions, the results were nondimensionalized by using airplane response factors. The metric is simple to implement and yet captures the first-order effects of turbulence. It is a function of the nondimensional incremental gust amplitudes and lengths. The algorithm produces the estimated maximum and minimum accelerations at the aft cabin location. These parameters are thought to be a good measure of the hazard to turbulence although other measures such as equivalent fall height are also attractive. The metric was applied to a simulated gust field of a convective frontal system. A least-squares calculation of the amplitude for five different gust lengths (50 to 800 m) was used on the simulated gust field. The analysis showed that the highest accelerations occurred for the subject airplane when the gust lengths (for the present simulated gust field) are 100 to 50 m or less. A simulated gust field with a grid spacing of less than the current 25 m is needed to determine whether gust lengths shorter than 50 m produce higher accelerations. The analysis also showed that the estimated acceleration at the same point in the simulated turbulence field can be significantly different depending on the airplane's direction of flight.

The analysis also included a calculation of the motion of an unrestrained mass in the aft cabin to simulate the motion of an unbuckled passenger or flight attendant. This analysis showed that a victim's impact against the airplane interior could be equivalent to falling over 10 ft for gust amplitudes of 100 ft/s and gust lengths of 500 ft. Thus, from the standpoint of the hazard to unrestrained passengers, the 25-m grid spacing of the present simulated gust field is adequate.

References

1. Anon.: In-Flight Safety of Passengers and Flight Attendants Aboard Air Carrier Aircraft. NTSB-AAS-73-1, March 1973.

2. Stewart, Eric C.: A Study of Airline Passenger Susceptibility to Atmospheric Turbulence Hazards. AIAA Paper 2000-3978, Aug. 2000.

3. Stewart, Eric C.: A Sensor-Independent Gust Hazard Metric. AIAA Paper 2001-4135, Aug. 2001.

4. Proctor, Fred H.; Hamilton, David W.; and Bowles, Roland L.: Numerical Study of a Convective Turbulence Encounter. AIAA Paper 2002-0944, Jan. 2002.

5. Jones, Robert T.: *The Unsteady Lift of a Finite Wing*. NACA TN 682, 1939.

6. Phillips, William H.; and Kraft, Christopher C.: *Theoretical Study of Some Methods for Increasing the Smoothness of Flight Through Rough Air*. NACA TN 2416, 1951.

7. Fuller, J. R.: Evolution of Airplane Gust Loads Design Requirements. *J. of Airc.*, vol. 32, no. 2, March–April 1995.

8. Bass, Ellen J., et al.: Pilot Decision Aid Requirements for a Real-Time Turbulence Assessment System. *The Tenth International Symposium on Aviation Psychology*, Columbus, Ohio, May 2–6, 1999.

Table 1. Simulated Airplane Characteristics

Characteristic	Value
Weight, W	180 000 lb
Wing area, S_w	1951 ft^2
Zero lift drag coefficient of tail, $C_{Do,t}$	0.01
Tail lift curve slope, $C_{L\alpha,t}$	1.19/rad
Wing downwash on tail, $\frac{\partial \varepsilon}{\partial \alpha}$	0.50
Pitch moment of inertia, I_y	525 000 slug- ft^2
Efficiency factor of tail, k_t	0.1058
Elevator effectiveness, $k_{\delta e}$	0.5
x location of wing aerodynamic center, x_w	–1.44 ft
z location of wing aerodynamic center, z_w	0.0 ft
x location of tail aerodynamic center, x_t	–66.8 ft
z location of tail aerodynamic center, z_t	0.0 ft
x location of thrust, x_T	0.0 ft
z location of thrust, z_T	0.0 ft
Thrust inclination angle, ε	0.0°
Pitch gain in autopilot, k_θ	2.0 rad/rad
Pitch rate gain in autopilot, k_q	0.3 rad/(rad/s)
Altitude gain in autopilot, k_h	0.0001 rad/ft
Flexible tail spring constant, k	131 880 lb/ft
Flexible tail effective mass, m_e	371 slugs
Thrust, *Thrust*	17 117 lb
Trim angle of attack, α_{trim}	1.33°
Trim elevator angle, $\delta_{e,trim}$	–2.10°
Trim flexible tail deflection, y_{trim}	0.0295 ft
Flexible tail natural frequency, f	3 Hz
Flexible tail stiffness factor, R_s	0.02
Horizontal tail area, S_t	542 ft^2
Wing lift curve slope (linear range), $C_{L_{\alpha,w}}$	7.03/rad
Total lift curve slope (linear range), C_{L_α}	7.625/rad

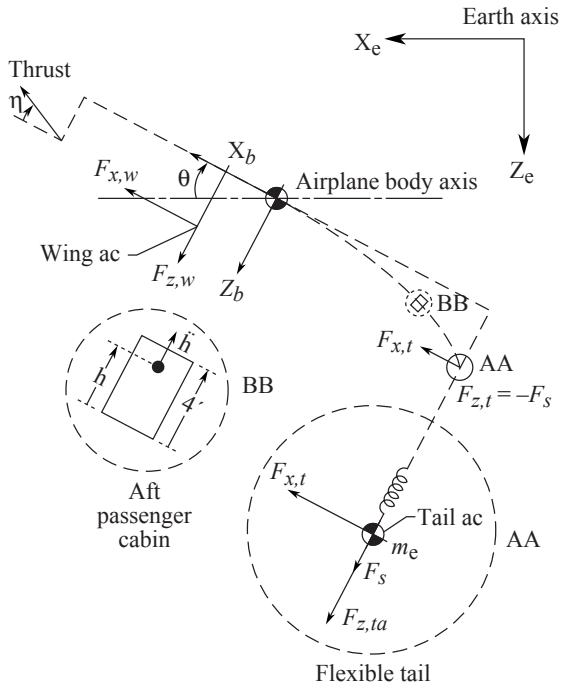

Figure 1. Axis systems.

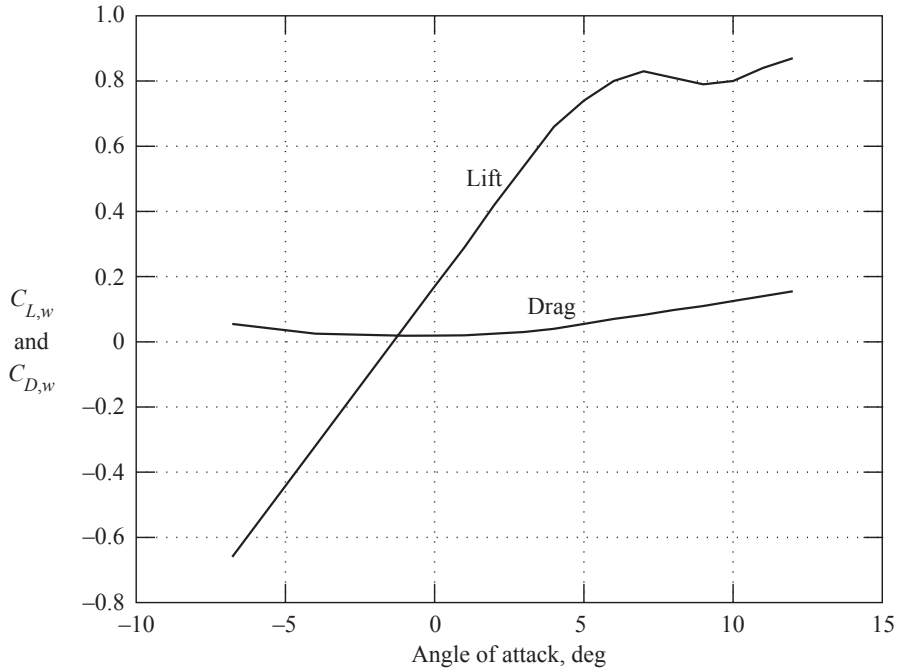

Figure 2. Aerodynamic characteristics of wing.

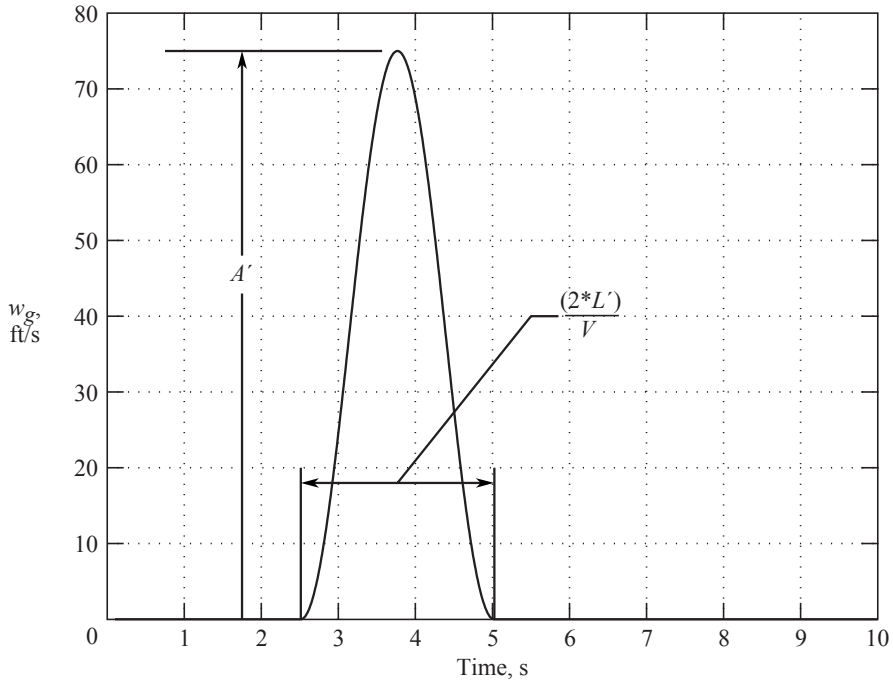

Figure 3. 1-cosine gust profile. A' = 75 ft/s, L' = 1000 ft, V = 796 ft/s.

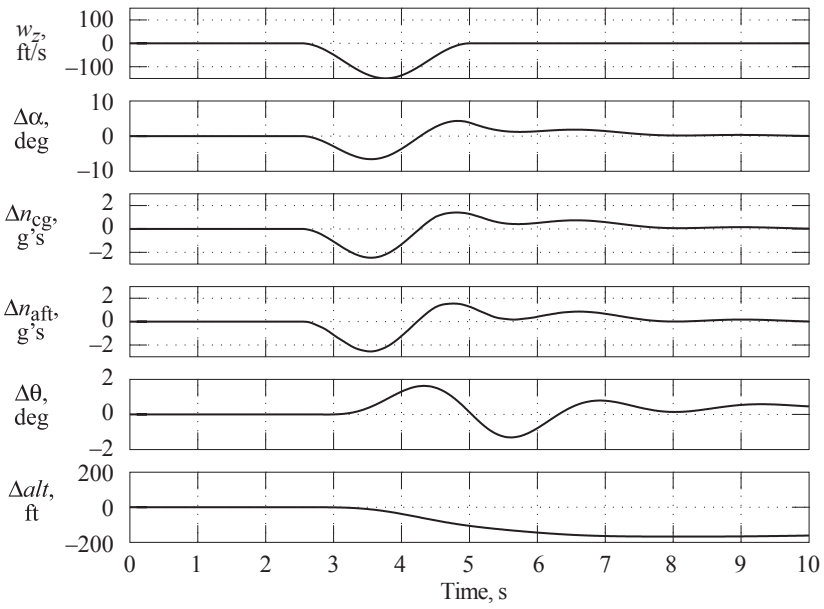

(a) Airplane states.

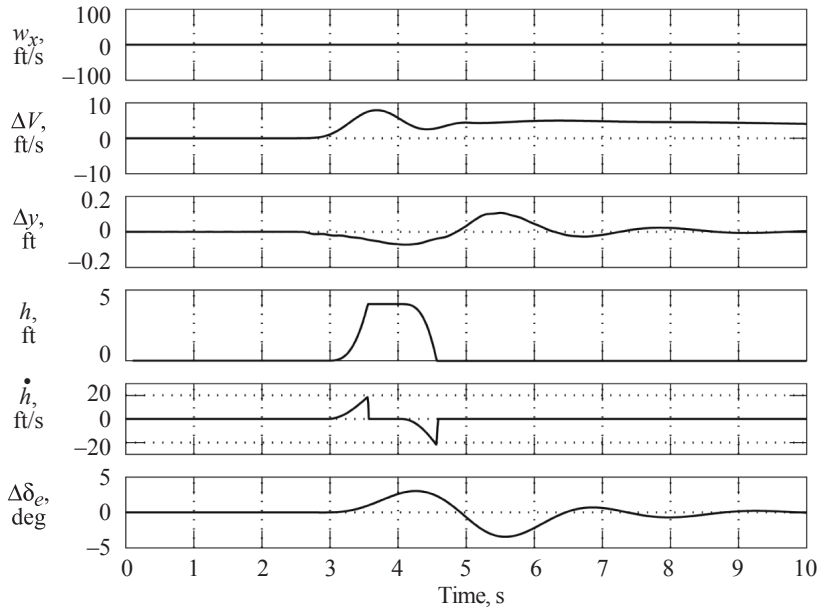

(b) Airplane and unrestrained mass states.

Figure 4. Time histories of airplane and unrestrained mass for downward 1-cosine gust. $A' = -150$ ft/s, $L' = 1000$ ft.

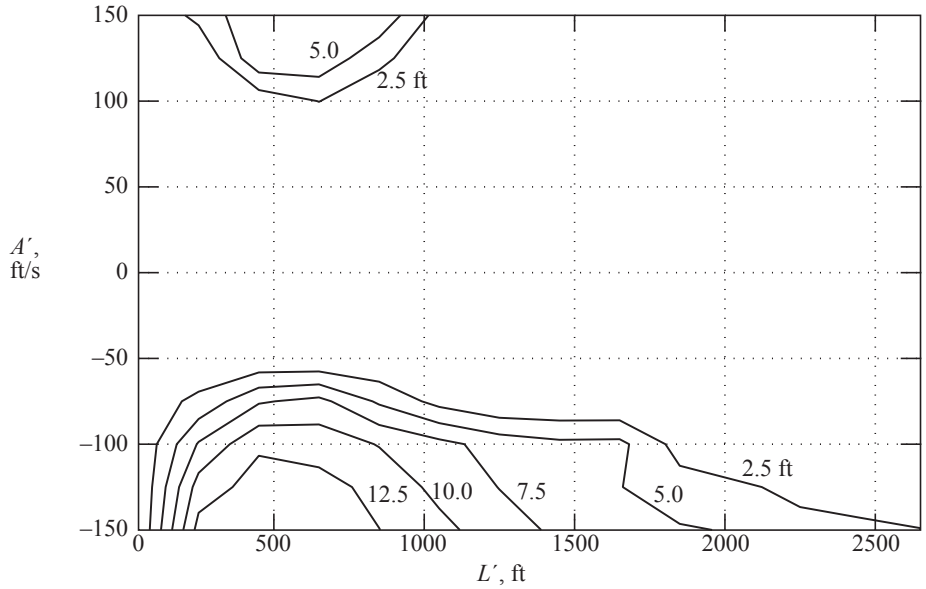

Figure 5. Contours of equivalent fall heights of unrestrained mass in aft cabin for 1-cosine gusts of various gust lengths and amplitudes.

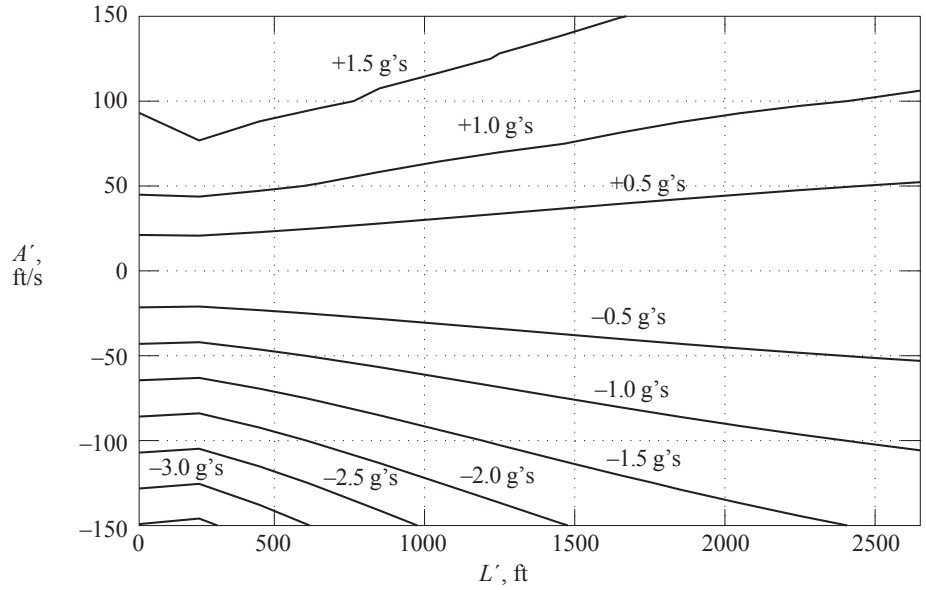

Figure 6. Contours of peak c.g. acceleration response to 1-cosine gusts of various gust lengths and amplitudes.

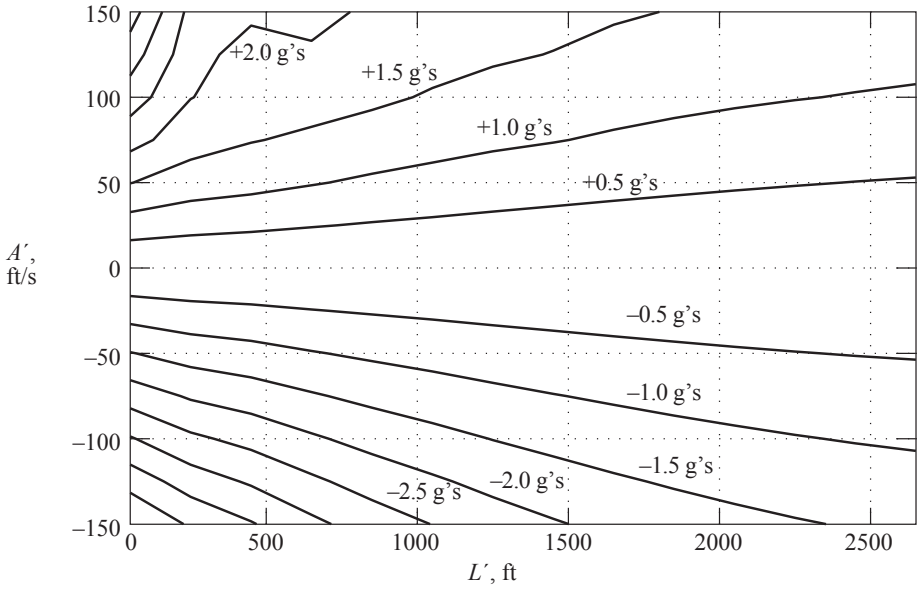

Figure 7. Contours of peak aft cabin acceleration response to 1-cosine gusts of various gust lengths and amplitudes.

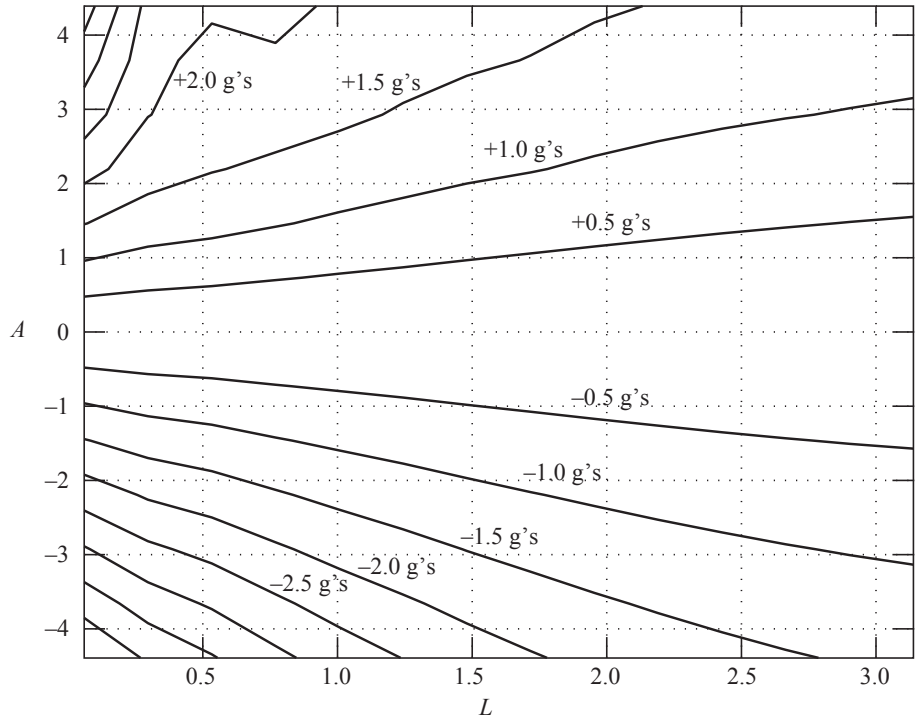

Figure 8. Contours of peak accelerations in aft cabin as function of nondimensional gust lengths and amplitudes. Gust amplitude factor = 34.15 ft/sec, gust length factor = 844.4 ft.

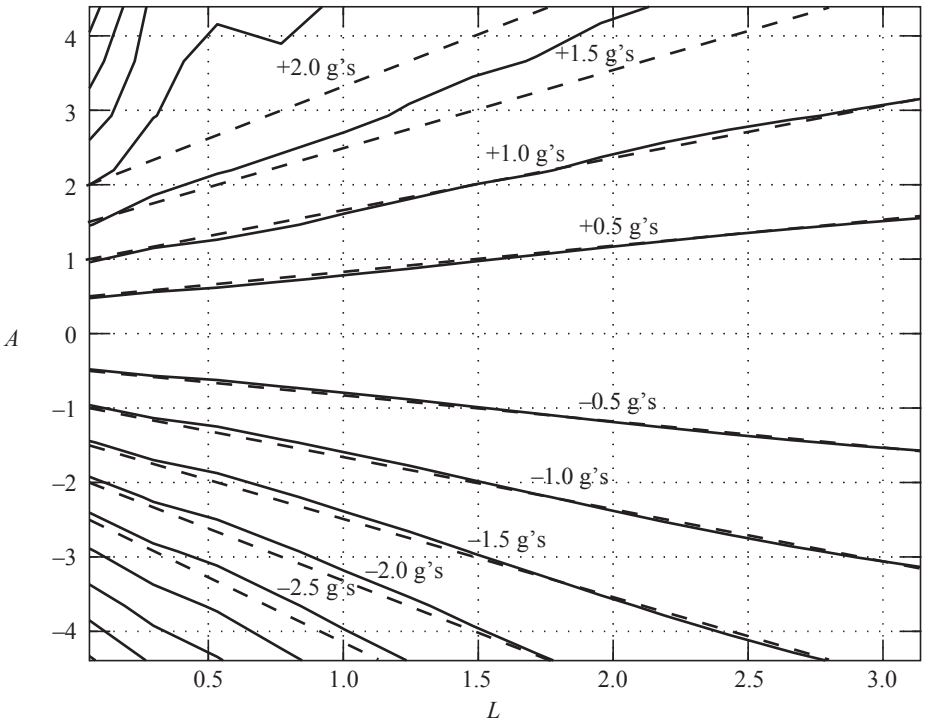

Figure 9. Comparison of curve fit used to define hazard metric and previous contours for aft cabin accelerations. Dotted lines are curve fit $A = 0.96 * a_n + 0.70 * a_n * L$.

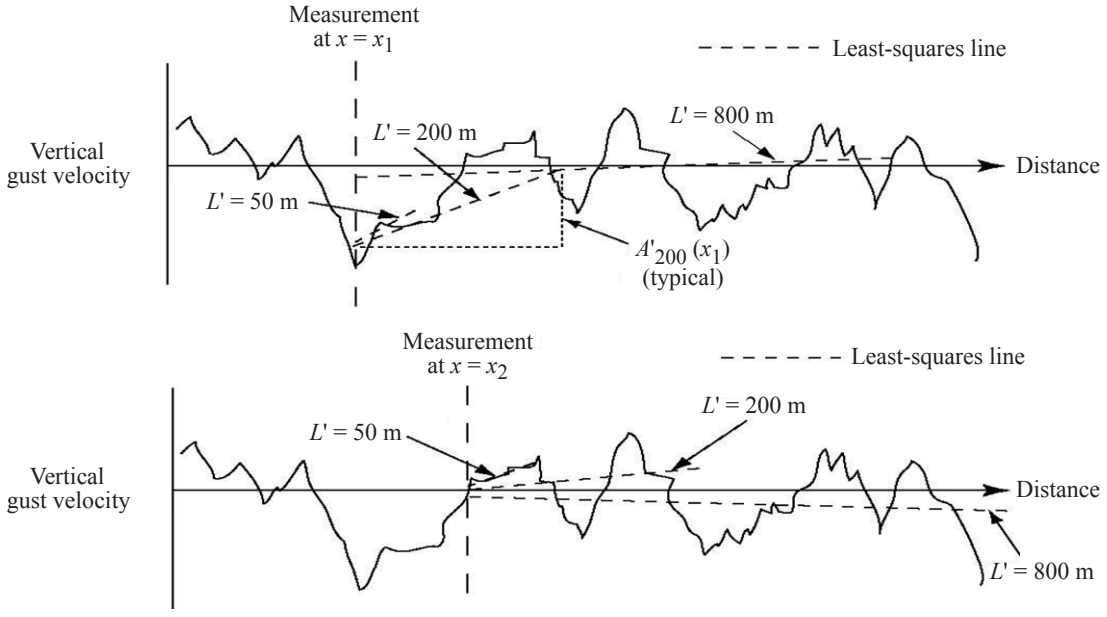

Figure 10. Illustration of method of calculating incremental gust amplitudes for 50-m, 200-m, and 800-m gust lengths using least-squares linear curve fit; 100-m and 400-m gust lengths omitted for clarity.

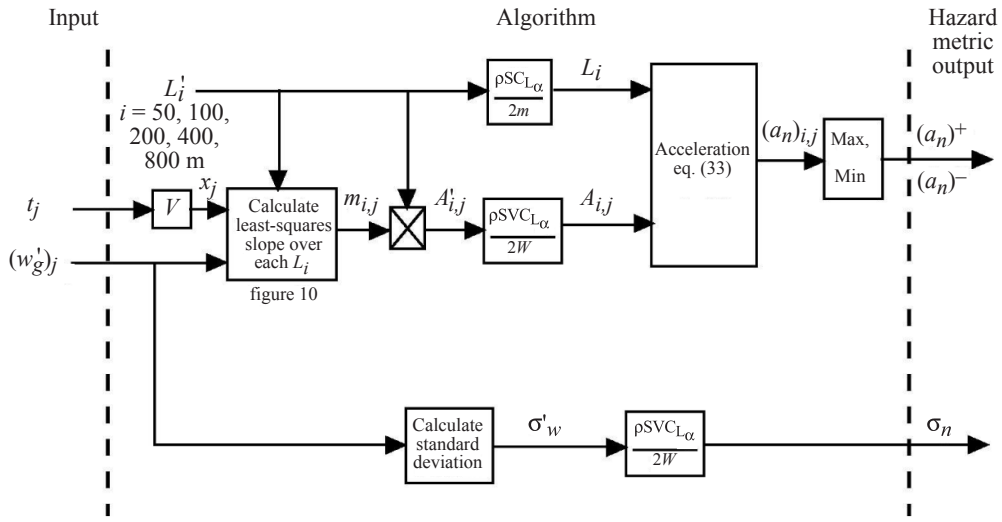

Figure 11. Flow diagram for operational hazard metric algorithm.

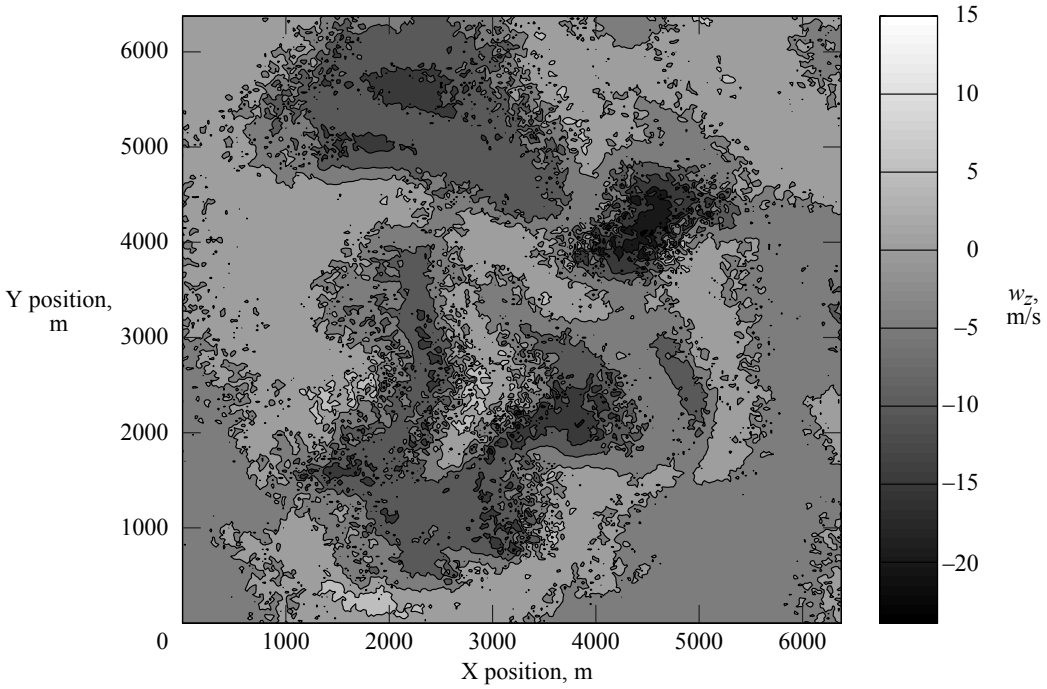

Figure 12. Contours of vertical winds (meter/second) from CFD simulation of convective frontal system (ref. 4).

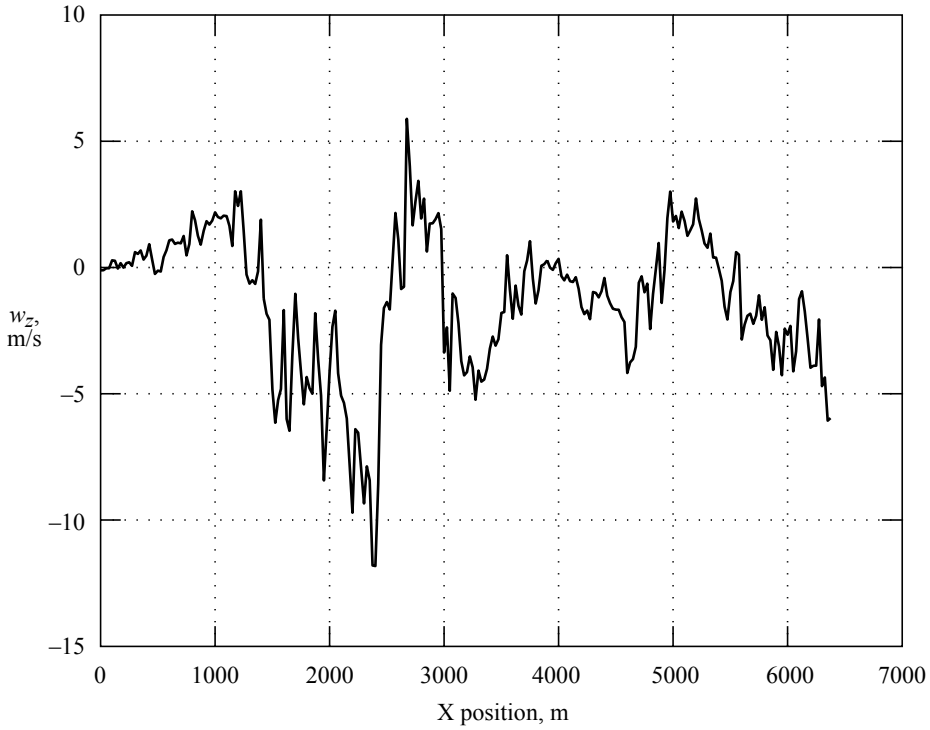

(a) Line y = 3200 m.

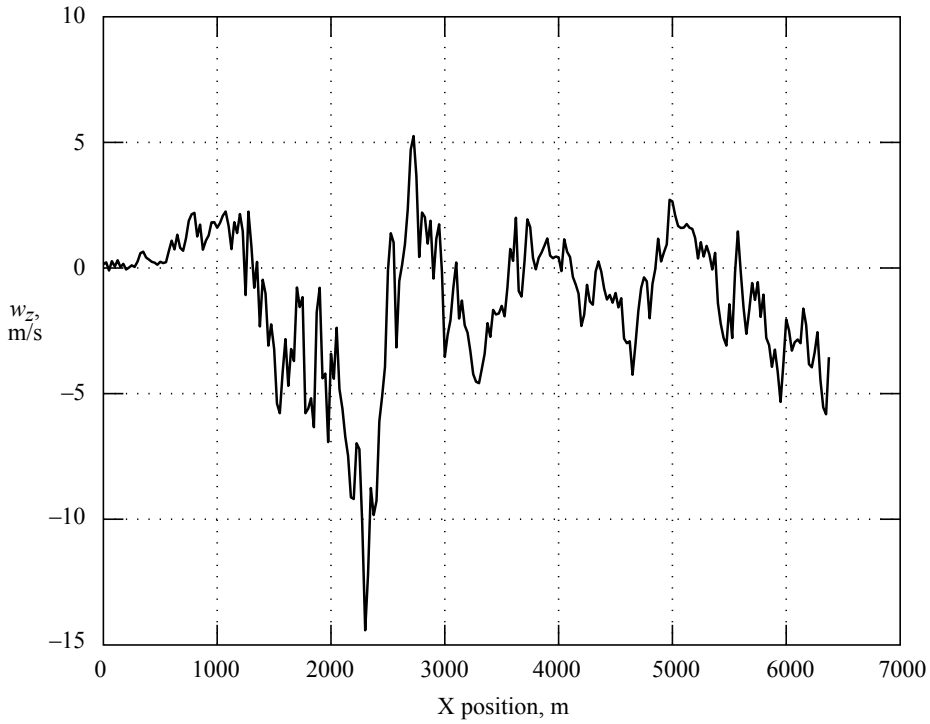

(b) Line y = 3225 m.

Figure 13. Vertical winds along two horizontal lines in figure 12.

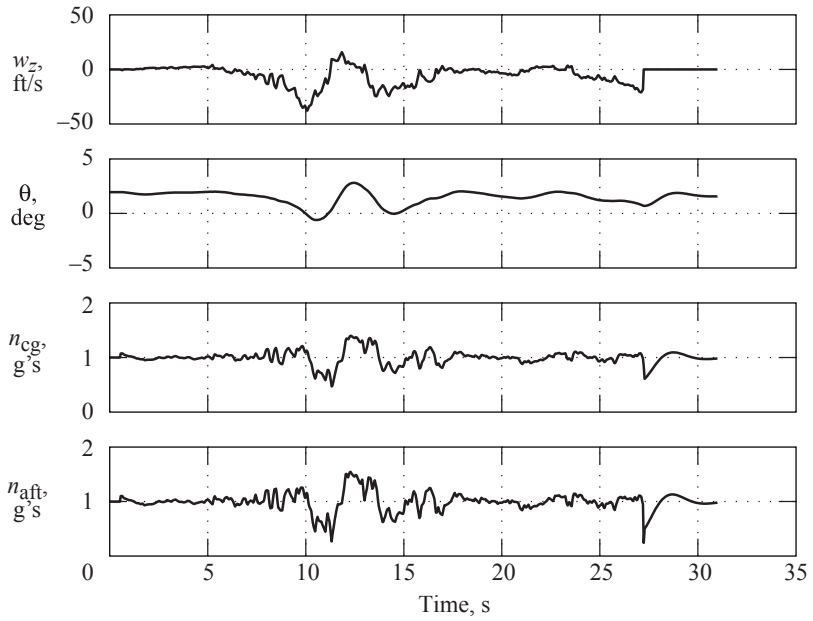

Figure 14. Real time simulation time history for trajectory approximately along straight line used in figure 13(a), y = 3200 m.

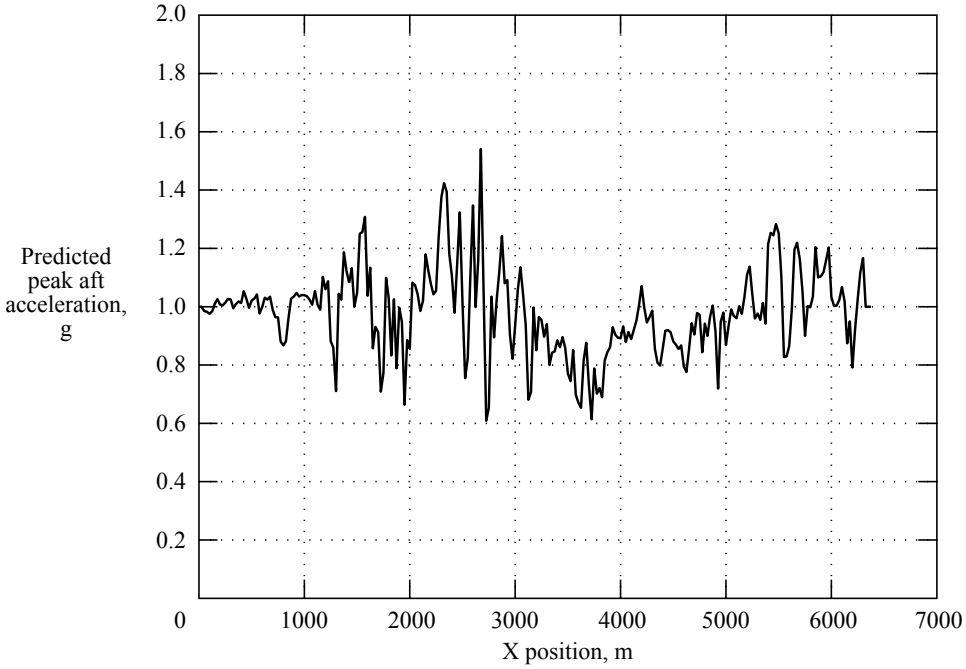

Figure 15. Peak accelerations calculated using curve fit for hazard metric using gust length of 100 m.

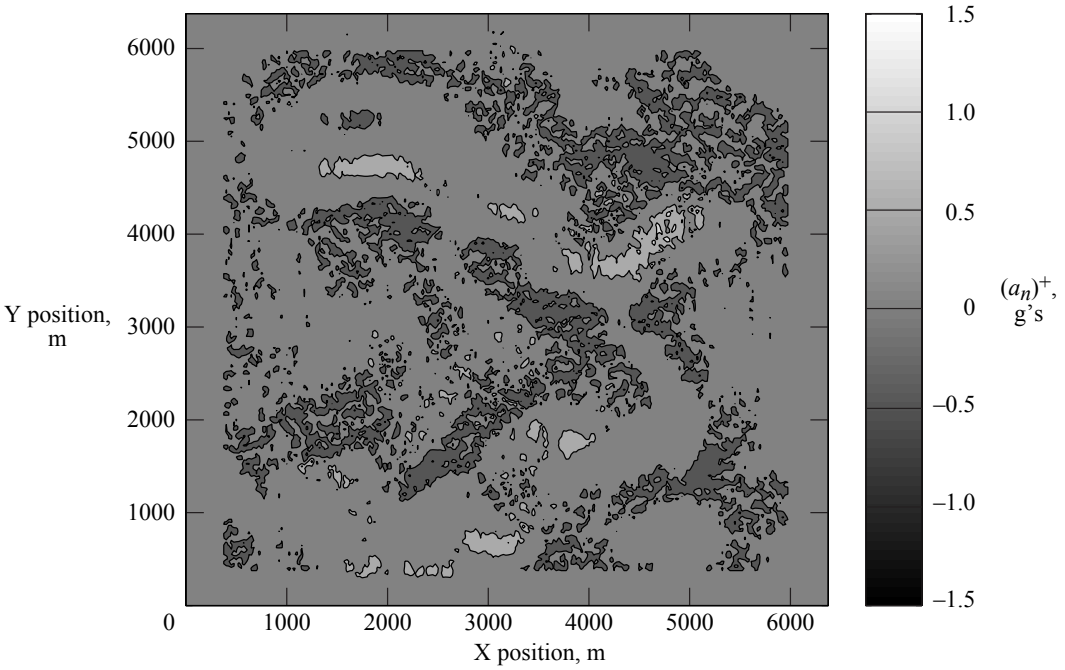

(a) Maximum acceleration. Peak value = +1.50 g's.

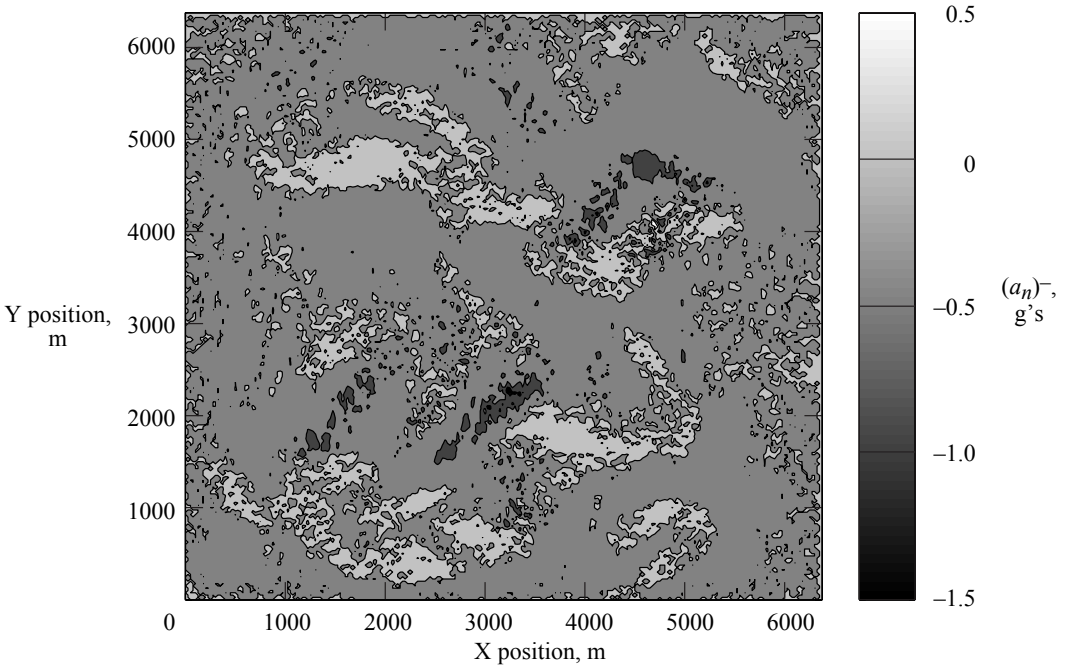

(b) Minimum acceleration. Peak value = –1.78 g's.

Figure 16. Peak acceleration contours for all five gust lengths combined.

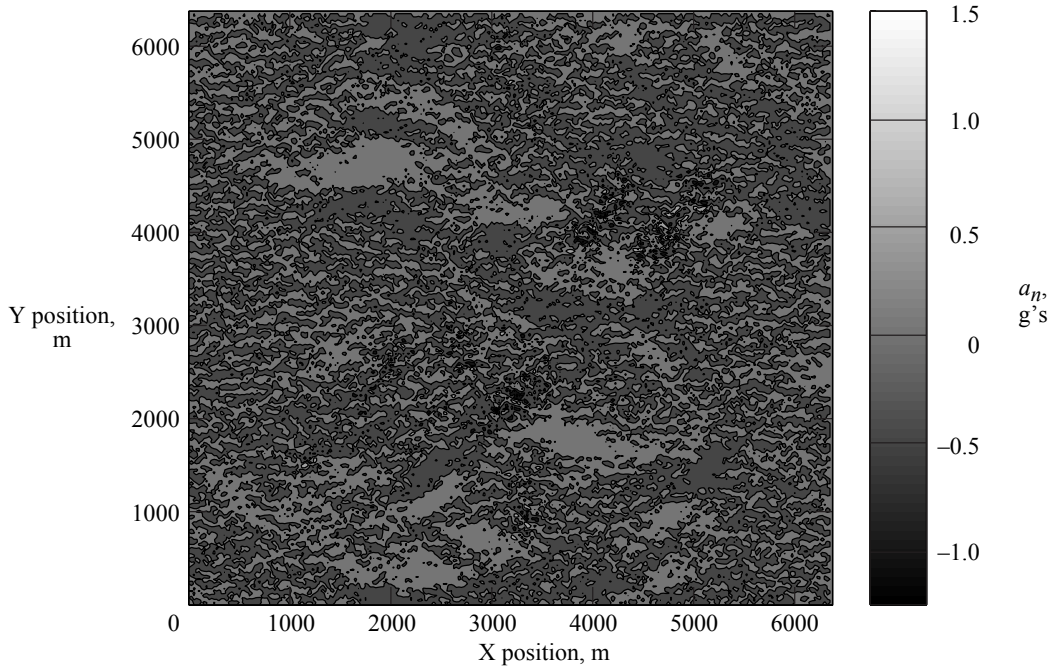

(a) L' = 50 m. Peak values = +1.50 g's and –1.25 g's.

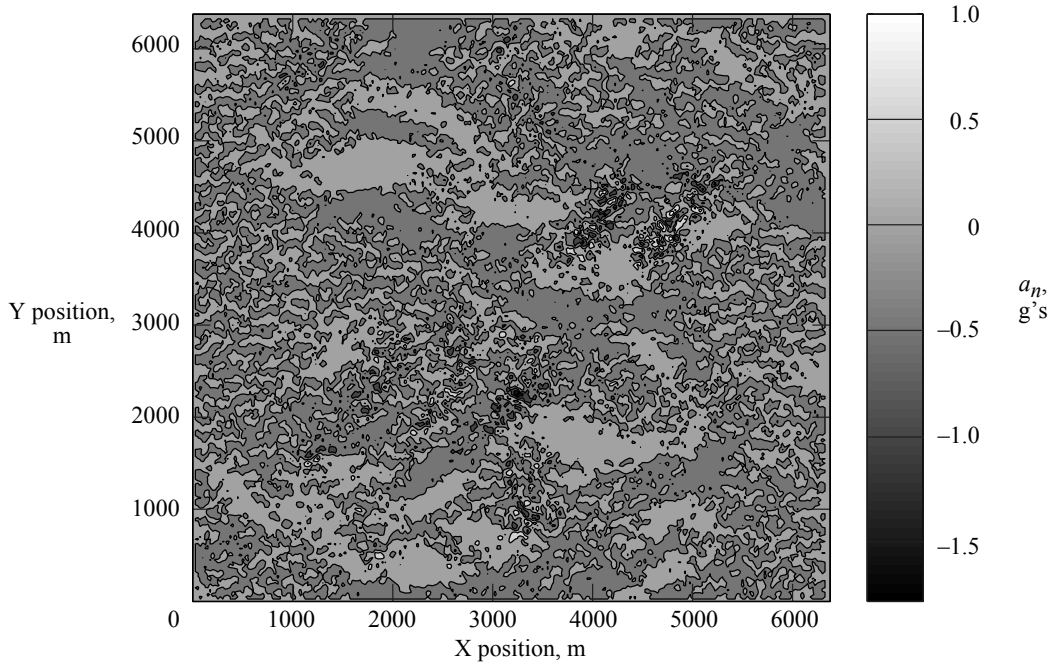

(b) L' = 100 m. Peak values = +1.42 g's and –1.78 g's.

Figure 17. Peak acceleration contours for individual gust lengths.

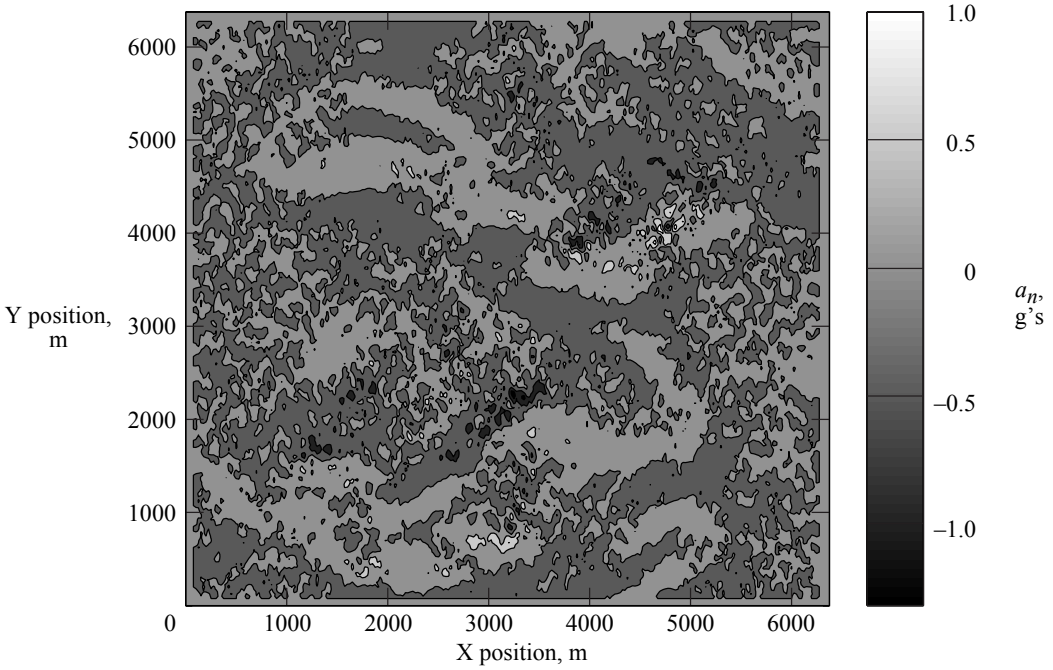

(c) L' = 200 m. Peak values = +1.26 g's and –1.32 g's.

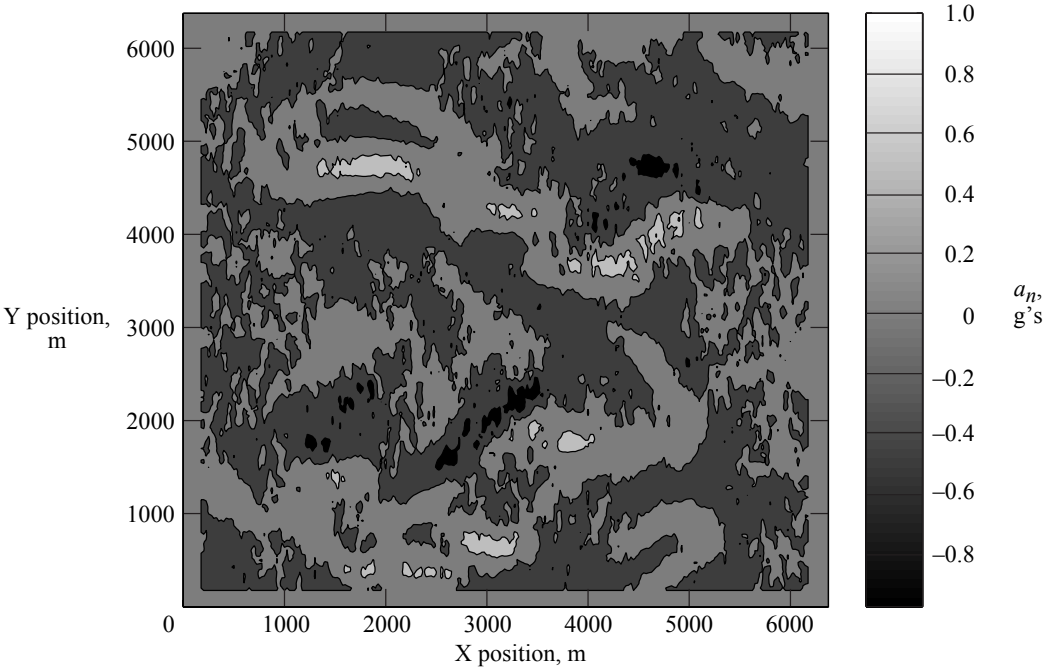

(d) L' = 400 m. Peak values = +1.02 g's and –0.98 g's.

Figure 17. Continued.

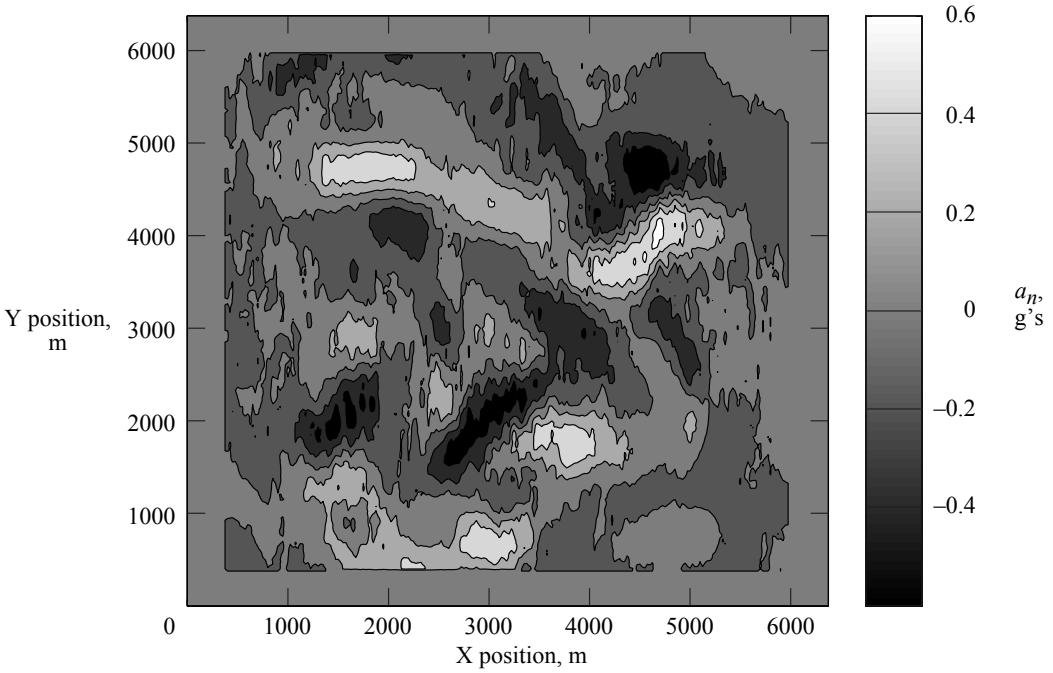

(e) L' = 800 m. Peak values = +0.73 g's and –0.60 g's.

Figure 17. Concluded.

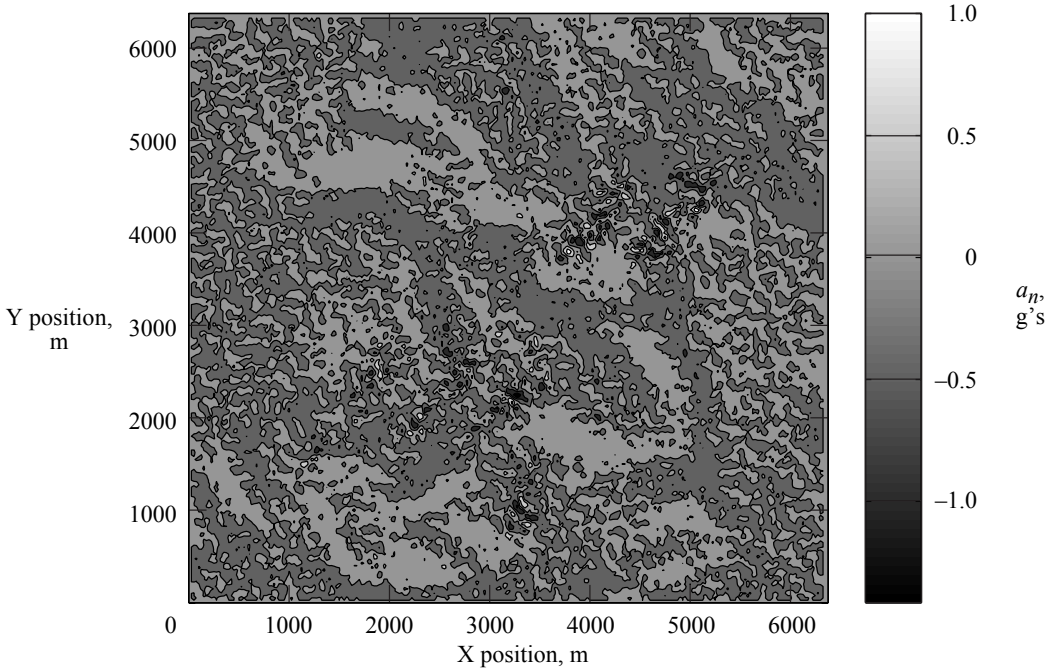

(a) Heading of 30°. Peak values = +1.27 g's and –1.41 g's.

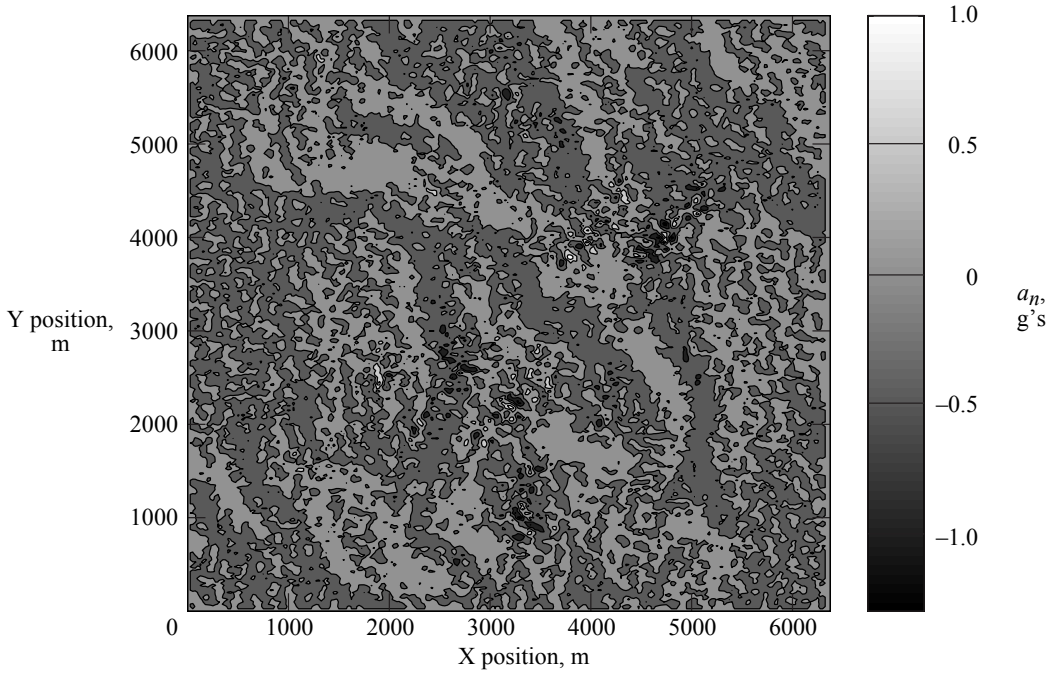

(b) Heading of 60°. Peak values = +1.29 g's and –1.30 g's.

Figure 18. Peak acceleration contours with L' = 100 m and different headings.

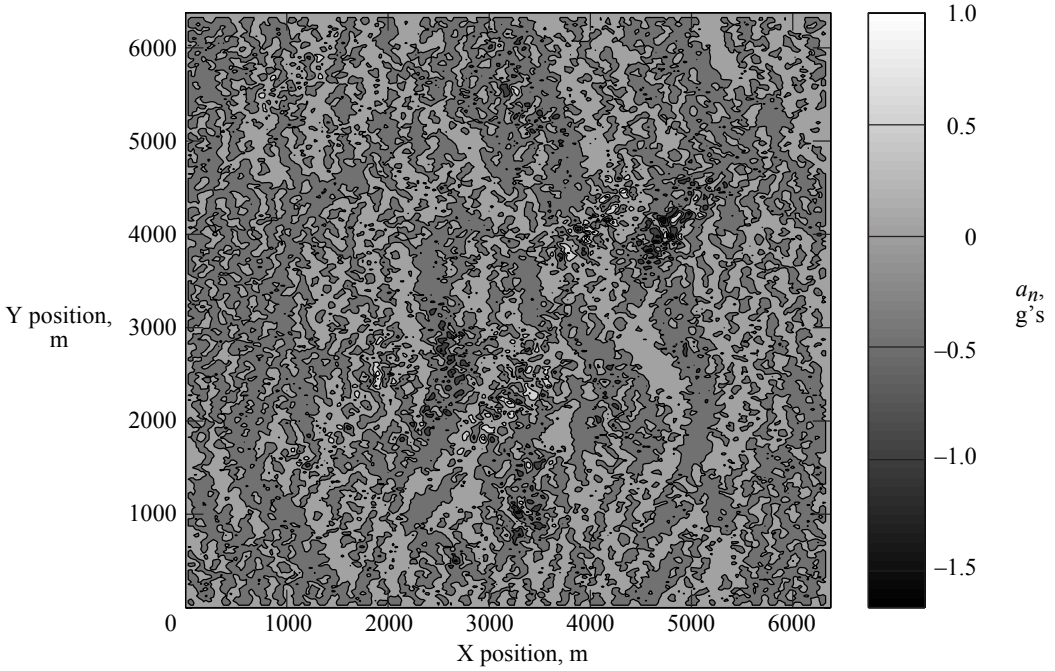

(c) Heading of 90°. Peak values = +1.45 g's and –1.67 g's.

Figure 18. Concluded.

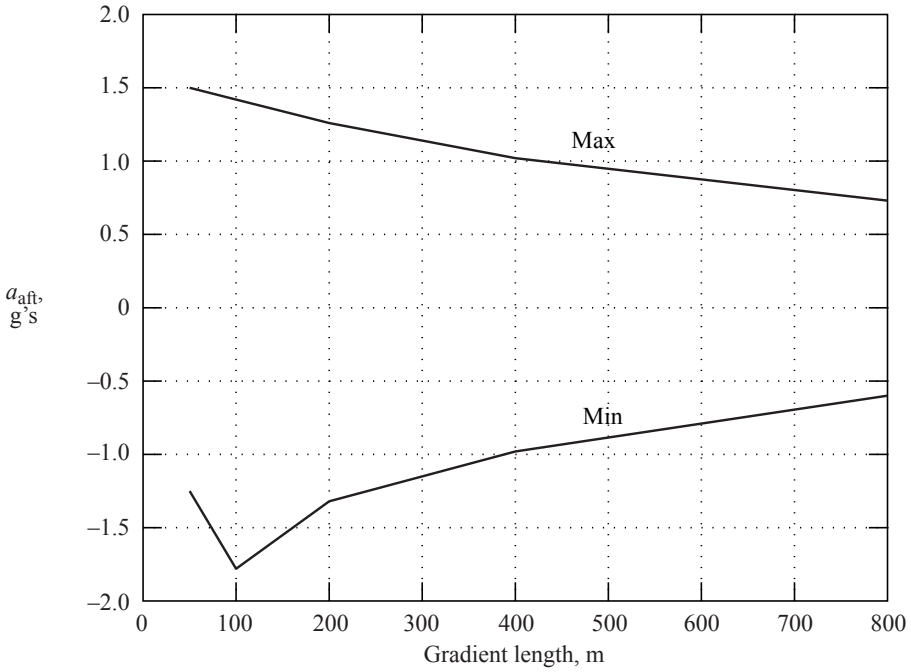

Figure 19. Peak accelerations as function of gust length for simulated gust field.

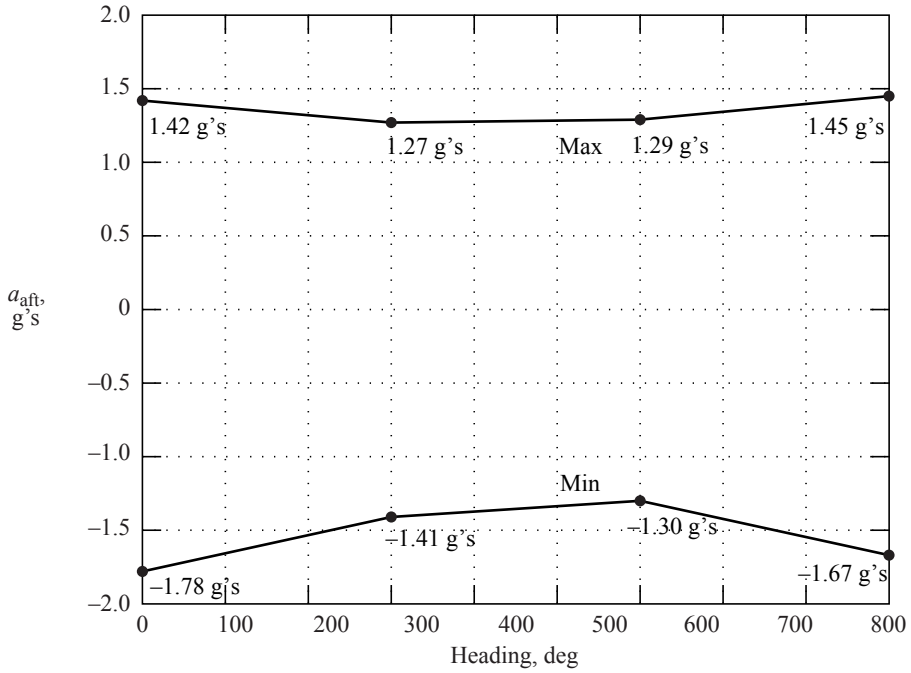

Figure 20. Peak accelerations as function of heading for gust length of 100 m.

REPORT DOCUMENTATION PAGE

Form Approved
OMB No. 0704-0188

1. REPORT DATE *(DD-MM-YYYY)*	2. REPORT TYPE	3. DATES COVERED *(From - To)*
01- 02 - 2005	Technical Publication	

4. TITLE AND SUBTITLE

Turbulence Hazard Metric Based on Peak Accelerations for Jetliner Passengers

5a. CONTRACT NUMBER

5b. GRANT NUMBER

5c. PROGRAM ELEMENT NUMBER

6. AUTHOR(S)

Stewart, Eric C.

5d. PROJECT NUMBER

5e. TASK NUMBER

5f. WORK UNIT NUMBER

23-728-40-30

7. PERFORMING ORGANIZATION NAME(S) AND ADDRESS(ES)

NASA Langley Research Center
Hampton, VA 23681-2199

8. PERFORMING ORGANIZATION REPORT NUMBER

L-18382

9. SPONSORING/MONITORING AGENCY NAME(S) AND ADDRESS(ES)

National Aeronautics and Space Administration
Washington, DC 20546-0001

10. SPONSOR/MONITOR'S ACRONYM(S)

NASA

11. SPONSOR/MONITOR'S REPORT NUMBER(S)

NASA/TP-2005-213528

12. DISTRIBUTION/AVAILABILITY STATEMENT

Unclassified - Unlimited
Subject Category 03
Availability: NASA CASI (301) 621-0390

13. SUPPLEMENTARY NOTES

Stewart, Langley Research Center, Hampton, VA.
An electronic version can be found at http://ntrs.nasa.gov

14. ABSTRACT

Calculations are made of the approximate hazard due to peak normal accelerations of an airplane flying through a simulated vertical wind field associated with a convective frontal system. The calculations are based on a hazard metric developed from a systematic application of a generic math model to 1-cosine discrete gusts of various amplitudes and gust lengths. The math model simulates the three degree-of-freedom longitudinal rigid body motion to vertical gusts and includes (1) fuselage flexibility, (2) the lag in the downwash from the wing to the tail, (3) gradual lift effects, (4) a simplified autopilot, and (5) motion of an unrestrained passenger in the rear cabin. Airplane and passenger response contours are calculated for a matrix of gust amplitudes and gust lengths. The airplane response contours are used to develop an approximate hazard metric of peak normal accelerations as a function of gust amplitude and gust length. The hazard metric is then applied to a two-dimensional simulated vertical wind field of a convective frontal system. The variations of the hazard metric with gust length and airplane heading are demonstrated.

15. SUBJECT TERMS

Atmospheric turbulence; Turbulence; Flight hazards; Aircraft loads

16. SECURITY CLASSIFICATION OF:			17. LIMITATION OF ABSTRACT	18. NUMBER OF PAGES	19a. NAME OF RESPONSIBLE PERSON
a. REPORT	b. ABSTRACT	c. THIS PAGE			STI Help Desk (email: help@sti.nasa.gov)
					19b. TELEPHONE NUMBER *(Include area code)*
U	U	U	UU	37	(301) 621-0390